Microstructural tectonometamorphic processes and the development of gneissic layering: a mechanism for metamorphic segregation

M. L. WILLIAMS,[1] E. A. MELIS,[1] C. F. KOPF[1] AND S. HANMER[2]
[1]*Department of Geosciences, University of Massachusetts, Amherst, MA 01003, USA (mlw@geo.umass.edu), and* [2]*Continental Geoscience Division, Geological Survey of Canada, Ottawa, Ontario, Canada*

ABSTRACT

The Mary granite, in the East Athabasca mylonite triangle, northern Saskatchewan, provides an example and a model for the development of non-migmatitic gneissic texture. Gneissic compositional layering developed through the simultaneous evolution of three microdomains corresponding to original plagioclase, orthopyroxene and matrix in the igneous rocks. Plagioclase phenocrysts were progressively deformed and recrystallized, first into core and mantle structures, and ultimately into plagioclase-rich layers or ribbons. Garnet preferentially developed in the outer portions of recrystallized mantles, and, with further deformation, produced garnet-rich sub-layers within the plagioclase-rich gneissic domains. Orthopyroxene was replaced by clinopyroxene and garnet (and hornblende if sufficient water was present), which were, in turn, drawn into layers with new garnet growth along the boundaries. The igneous matrix evolved through a number of transient fabric stages involving S-C fabrics, S-C-C′ fabrics, and ultramylonitic domains. In addition, quartz veins were emplaced and subsequently deformed into quartz-rich gneissic layers. Moderate to highly strained samples display extreme mineralogical (compositional) segregation, yet most domains can be directly related to the original igneous precursors. The Mary granite was emplaced at approximately 900 °C and 1.0 GPa and was metamorphosed at approximately 750 °C and 1.0 GPa. The igneous rocks crystallized in the medium-pressure granulite field (Opx–Pl) but were metamorphosed on cooling into the high-pressure (Grt–Cpx–Pl) granulite field. The compositional segregation resulted from a dynamic, mutually reinforcing interaction between deformation, metamorphic and igneous processes in the deep crust. The production of gneissic texture by processes such as these may be the inevitable result of isobaric cooling of igneous rocks within a tectonically active deep crust.

Key words: gneiss; granulite; lower crust; metamorphic segregation.

INTRODUCTION

Gneisses are coarse-grained, compositionally layered metamorphic rocks. They make up a significant proportion of exposed continental crust, particularly in Archean cratons, and they are believed to be a dominant component of the lower crust (Rudnick & Fountain, 1995). Understanding the origin of gneisses is important for understanding deep crustal processes and for evaluating the evolution of these processes through Earth history. A variety of models has been proposed for the development of gneissic texture including: (1) models in which compositional layering results from metamorphism and/or transposition of an originally layered protolith (Myers, 1978; Davidson, 1984; Jordan, 1988); (2) models in which igneous magma, whether internally or externally derived, is an important component of the gneissic layering (Johannes, 1983; Lucas & St. Onge, 1995); and (3) models involving metamorphic segregation or differentiation, e.g. the solid-state segregation and concentration of specific minerals into layers (Robin, 1979; Van der Molen, 1985). This final process, perhaps the most poorly understood of the three, is the subject of this paper.

The process of metamorphic differentiation has been recognized for many years (Turner, 1941; Ramberg, 1952; Turner & Verhoogen, 1960; Misch, 1968). However, the actual mechanisms that produce the mineralogical or compositional segregation are still unclear. Some workers have considered the process to be primarily a deformational one, whereby layering reflects differences in mechanical behaviour (brittle or ductile) during deformation, or differential solubility due to concentration of stress or strain energy (Ramberg, 1952; Turner & Verhoogen, 1960; Van der Molen, 1985). Others have seen the process as a dominantly metamorphic one, with compositional or mineralogical segregation resulting from chemical potential gradients caused by grain boundary effects or local pressure differences (Ramberg, 1952; Bowes & Park, 1966; Spry, 1969; Yardley, 1989). In most gneisses, segregation probably involves some combination of deformation and metamorphic (or metasomatic) processes (Robin, 1979; Van der Molen, 1985), but detailed examples and documented mechanisms are rare in the literature.

The Mary granite[1], northern Saskatchewan, provides a well-exposed example of at least one variety of

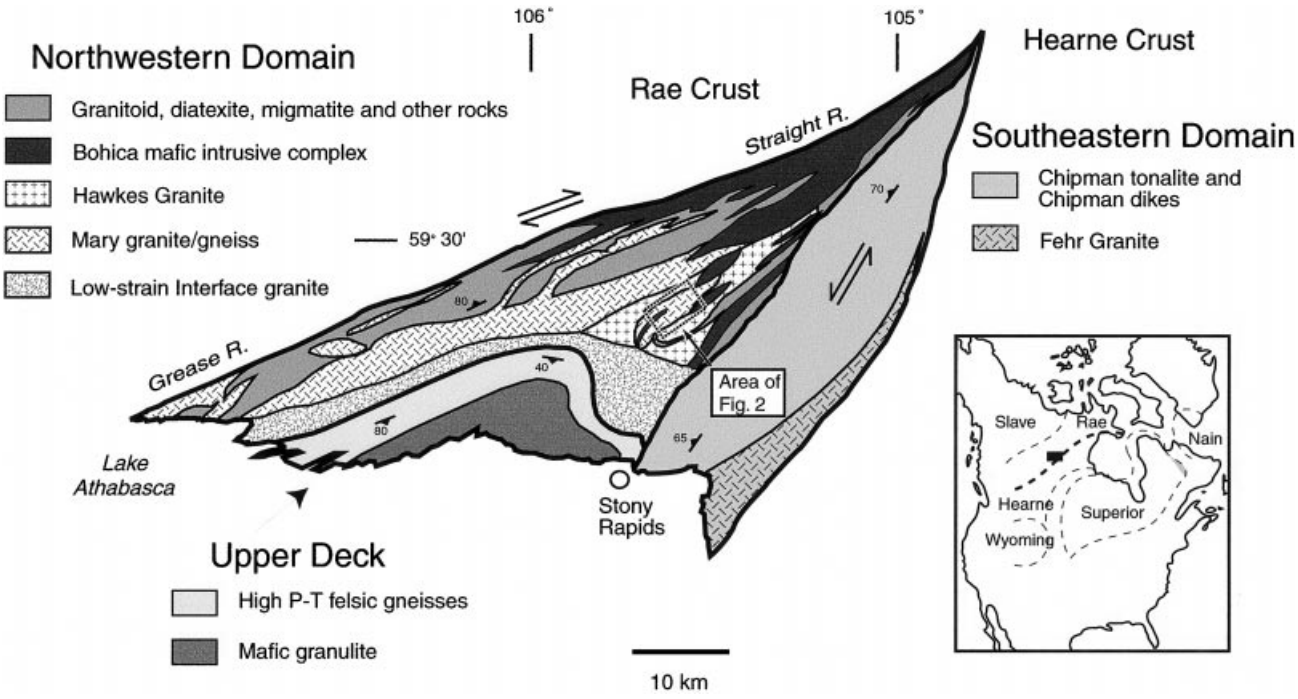

Fig. 1. Generalized geological map of the East Athabasca mylonite triangle (EAmt) (modified from Hanmer *et al*., 1994; Hanmer, 1994). Inset shows the location of the EAmt along the Snowbird Tectonic Zone (Hoffman, 1988). Dotted box shows the location of Fig. 2.

non-migmatitic gneissic texture. A complete gradation can be observed from essentially undeformed Opx-bearing granite to strongly layered granulite facies Cpx–Grt–Pl gneiss (abbreviations after Kretz, 1983). The textural transition resulted from an interplay of deformational processes (both brittle and ductile) and metamorphism, especially the localized growth of reaction products on specific reactants. The compositional segregation process was extremely effective, and yet, even in the most highly deformed rocks, it is possible to broadly relate textural components of the gneiss to original igneous minerals or textural domains. The purpose of this paper is to document the textural transition and to interpret the microscale processes that led to the development of compositional layering. The model may be applicable to a large class of gneisses, and it provides insight into the complex relationship between deformation and metamorphism during high-grade deep crustal tectonism.

GEOLOGICAL SETTING

The Striding-Athabasca mylonite zone (Hanmer & Kopf, 1993; Hanmer *et al*., 1994) is a 400 km long segment of the Snowbird tectonic zone, the geophysically defined boundary between the Rae and Hearne Archean crustal domains in Canada (Goodacre *et al*., 1987; Hoffman, 1988). The Striding-Athabasca mylonite zone is particularly well exposed in the East Athabasca mylonite triangle (EAmt), at the eastern end of Lake Athabasca, Saskatchewan (Fig. 1). There, a 40 km-wide zone of anastomosing granulite facies mylonites is separated from the Rae (north-west) and Hearne (south-east) Province wall rocks by narrow greenschist facies shear zones (Hanmer, 1994; Hanmer *et al*., 1992, 1994).

The EAmt can be divided into three structural/tectonic domains (Fig. 1). All three have shallowly plunging, north-east-trending mineral lineations, and were deformed under granulite facies conditions at approximately 2.6 Ga (Hanmer *et al*., 1994). The southern domain, or upper deck, is dominated by mafic granulite and leucocratic gneiss (Hanmer *et al*., 1992, 1994; Kopf *et al*., 1997). Parts of this domain experienced a phase of high-T, very high-P metamorphism (1000 °C, >1.6 GPa) before juxtaposition with the other domains (Snoeyenbos *et al*., 1995). The south-eastern domain is dominated by the Chipman tonalite and the Chipman dyke swarm and shows evidence for tectonism at both 3.2 and 2.6 Ga (Williams *et al*., 1995). The north-western domain is dominated by felsic to mafic plutonic rocks, including the Mary granite. It has a vertical foliation and sub-horizontal mineral lineation with abundant dextral strike–slip shear sense indicators. Our model for the tectonic history of the EAmt involves *c*. 3.2 Ga deformation and granulite facies metamorphism, possibly in an

[1]The name Mary granite was used by Hanmer *et al*. (1994) and on the geological map of the EAmt (Hanmer, 1994) and so will be retained here. However, except for lowest-strain exposures, most exposures display at least microscale compositional gneissic layering.

arc-related setting, and a second phase of granulite facies deformation and metamorphism at 2.6 Ga in an intra-continental, transpressional shear zone (Hanmer *et al*., 1994, 1995). This second phase apparently established the present configuration of the three domains. A final metamorphic and deformational event, at *c*. 1.9 Ga, is recorded in the wall rocks, but apparently did not produce significant deformation within the EAmt; the EAmt may have been at a shallower crustal level or may have acted as a relatively rigid refractory domain during this younger event.

The Mary granite is associated with the Reeve diatexite, the Bohica mafic complex, and several other felsic granitoids, all in the north-western domain of the EAmt (Fig. 1) (Hanmer, 1994). The Reeve diatexite is a deformed (mylonitized) migmatite. The 2.62 Ga Bohica mafic complex is a heterogeneous assemblage of deformed and metamorphosed norite, gabbro and diorite (Hanmer *et al*., 1994). Several other relatively felsic, garnetiferous granitoids have been distinguished from the Mary granite in the field, including the Hawkes granite (Fig. 1) (Hanmer, 1994), but based on the similarity in age, composition and deformational character, these will be included here under the general name Mary granite.

GEOLOGICAL CHARACTERISTICS OF THE MARY GRANITE

The 2.620–2.605 Ga (Hanmer *et al*., 1994) Mary granite is the largestcoherent granite body in the EAmt and comprises much of the north-western, structural domain (Fig. 1). In general, the Mary granite is penetratively foliated and mylonitized, although small volumes of coarse plutonic protolith are locally exposed. Typical exposures exhibit white streaks and ribbons of polycrystalline feldspar separated by a finer matrix of feldspar, quartz and various amounts of hornblende, blood-red garnet, clinopyroxene, orthopyroxene and ilmenite. Biotite is extremely rare. In low-strain domains, it can be seen that more strongly deformed components are cut by less strongly deformed equivalents indicating that the granite is generally syntectonic with respect to the 2.6 Ga granulite facies deformation (Hanmer *et al*., 1994). Throughout the following discussion, we use the terms 'gneiss' and 'gneissic' because the Mary granite contains well-developed mineralogical layering; we also use the term mylonite because individual layers commonly show evidence for strong ductile deformation including intense foliation, lineation and monoclinic fabric elements (Passchier & Trouw, 1996).

One of the most striking characteristics of the Mary granite is its broad range of deformational and metamorphic textures. Individual outcrop exposures display a range from medium- to coarse-grained igneous textures with no visible foliation or lineation, to strongly compositionally banded gneisses to S-C-C′ mylonites to fine-grained ultramylonites. Some of the variation reflects progressive phases of granite emplacement relative to the accumulating regional strain. However, other textural variations probably reflect heterogeneous strain within intrusive bodies. Continuous gradients from relatively undeformed granite to highly strained gneiss can be seen on scales from thin sections to map-scale. Granitoids in the vicinity of East and West Hawkes Lakes (i.e. Hawkes granite of Hanmer, 1994) show some of the most dramatic variations from isotropic, equigranular, medium-grained Opx-bearing plutonic rocks to ribbon S-C-C′ mylonite and locally to ultramylonite (Fig. 2).

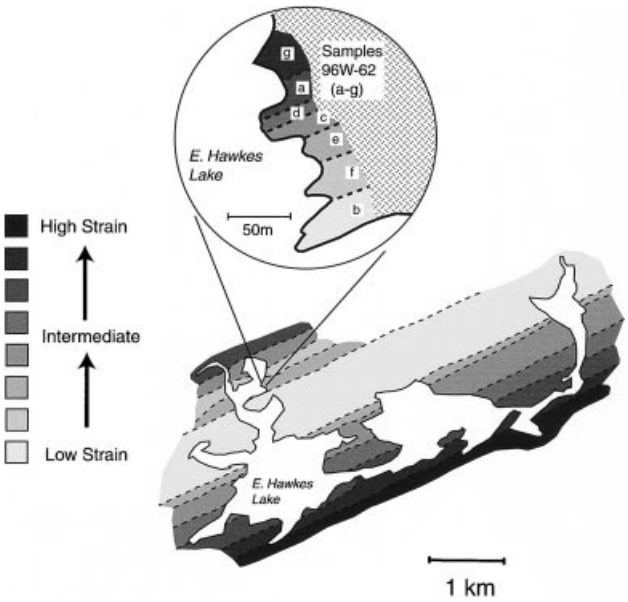

Fig. 2. Sketch map of East Hawkes Lake area, showing relative intensity of strain in Mary granite (Hawkes granite of Hanmer, 1994). Qualitative strain estimates are based on the relative intensity of fabric development in the field, particularly the degree of deformation and recrystallization of plagioclase porphyroblasts, orthopyroxene grain size reduction and matrix mylonitization. The relative intensities were checked using thin sections of samples from each domain. The inset shows local strain gradients that are present within many of the broader domains, and the locations of samples W62a–g.

Whole-rock compositions

Representative whole-rock compositions for samples of Mary granite throughout the EAmt are presented in Table 1. Based on major element composition, the rocks range from diorite to granite and most are formally granodiorite. The rocks are characterized by wide variation in SiO_2 from <60 to >70 wt%, and somewhat lesser variation in total alkali elements. We suspect that this compositional variation represents the original compositional range of the igneous magmas, perhaps involving mixing of mafic mantle-derived materials with crustally derived components. However, additional variation, particularly in SiO_2, may reflect additions of quartz in veins during deformation (see below).

No systematic variation in bulk composition is apparent with increasing intensity of gneissic fabric (Table 1). Seven samples (W62a–g) were collected from a single strain gradient at one outcrop on East Hawkes Lake (Fig. 2). Although the fabric varies from essentially undeformed to mylonitic gneiss, compositions are nearly identical except for one sample (W62g), which is neither the most nor the least intensely strained. We suspect that this sample represents an injection of a somewhat more mafic phase of the composite Mary granite.

Textural characteristics of low-strain samples

The least deformed samples of Mary granite contain quartz, plagioclase, K-feldspar, orthopyroxene (hypersthene), ilmenite and small amounts of hornblende, clinopyroxene, anthophyllite and chlorite. Three distinct grain sizes are apparent (Fig. 3a). The largest grains (to 2 mm) include plagioclase, orthopyroxene and K-feldspar. These megacrysts are set in a medium-grained matrix (to 0.5 mm) of quartz, plagioclase, K-feldspar and ilmenite. The finest grains (50–100 μm) are spherical to elliptical grains of quartz and

Table 1. Major and trace element analyses of selected Mary granite samples.

	Regional samples						Samples from one locality (96W-)						
Sample	S182	C664a	C728	S230	C187	M190	62a	62b	62c	62g	63	66a	71
Location*	WH	ML	ML	TL	WH	C1	WH	WH	WH	WH	WH	WH	WH
SiO_2	69.70	66.20	62.90	62.80	69.93	64.50	69.09	69.52	69.15	59.24	70.73	62.93	74.14
TiO_2	0.50	0.71	0.84	0.90	0.60	0.88	0.53	0.55	0.58	1.25	0.46	0.82	0.39
Al_2O_3	13.80	14.80	15.80	14.80	13.22	14.91	14.11	13.79	13.80	15.47	13.80	14.78	12.70
Fe_2O_3T	5.20	6.90	8.80	9.40	4.98	7.86	5.14	5.31	5.46	10.66	4.43	9.12	3.04
Fe_2O_3	0.20	0.90	1.50	0.50	–	–	–	–	–	–	–	–	–
FeO	4.50	5.40	6.60	8.00	–	–	–	–	–	–	–	–	–
MnO	0.05	0.08	0.12	0.12	0.07	0.11	0.07	0.07	0.07	0.16	0.06	0.14	0.04
MgO	0.76	1.41	0.70	0.96	0.72	1.66	0.49	0.53	0.55	1.38	0.43	0.70	0.20
CaO	1.95	3.64	3.69	3.78	2.19	3.95	2.45	2.08	2.37	4.80	2.21	4.25	1.27
Na_2O	2.60	3.00	3.70	3.10	2.58	2.43	2.58	2.54	2.56	3.48	2.63	3.14	2.39
K2O	4.74	3.24	2.93	3.47	4.47	2.82	4.41	4.56	4.51	2.78	4.37	2.97	5.78
H2O	0.80	0.60	1.00	0.70	–	–	–	–	–	–	–	–	–
P_2O_5	0.15	0.22	0.23	0.26	0.17	0.20	0.16	0.16	0.17	0.41	0.14	0.26	0.10
Σ	99.75	100.20	100.01	99.39	98.92	99.32	99.03	99.10	99.21	99.62	99.25	99.11	100.04

plagioclase that decorate the grain boundaries of the coarser minerals. As discussed below, the largest two size classes are interpreted to be a remnant igneous texture; the finest grains are interpreted to be new minerals, produced by metamorphic reactions and local dynamic recrystallization along grain boundaries.

Blocky plagioclase megacrysts (up to 2 mm in length) are common in low-strain samples (Fig. 3a,b). Most have texturally distinct cores and rims. The cores have albite twinning and weak concentric zoning. Some albite twins are slightly bent, but undulatory extinction is uncommon. The rims have a different extinction angle than the cores; rims are more albitic. Boundaries between cores and rims are sharp and euhedral. The outer boundaries of the rims preserve the blocky shape of the megacrysts, but at high magnification are irregular, preserving equilibrium triple junction boundaries against matrix minerals (Fig. 3b). Myrmekitic and symplectitic intergrowths of quartz and plagioclase are common within and near the plagioclase rims. Locally, a narrow stringer of K-feldspar occurs between the symplectitic plagioclase and the rest of the megacryst. Although this may represent a metamorphic replacement of K-feldspar by plagioclase and quartz (Simpson & Wintsch, 1989), we interpret it to be an igneous texture recording resorption during thermal variations in the Mary granite magma. Some samples display a distinct alignment of plagioclase crystals that may represent an igneous flow foliation.

Orthopyroxene megacrysts are present, but orthopyroxene more commonly occurs in clusters associated with ilmenite and quartz (Figs 3a & 4a). The clusters are irregularly shaped, either wispy, triangular or ellipsoidal. They contain spherical crystals of ferrosilite (up to 0.5 mm) with finer quartz and ilmenite along grain boundaries. The orthopyroxene crystals have uniform extinction and display little evidence for ductile deformation. Instead, they contain abundant microfractures, generally along crystallographic cleavage planes, and show evidence for mechanical breaking and dispersal along the foliation. Orthopyroxene was probably an original constituent of the granitoids, but we are uncertain of the degree to which these grains have been modified after crystallization in the low-strain samples. The clusters may be fractured and slightly recrystallized igneous crystals or they may be reaction products, together with quartz and ilmenite, from an original pyroxene or other igneous mineral. For the purpose of this study, the Opx–Qtz–Ilm clusters represent starting components for the observed evolution toward gneissic texture. Knowledge of earlier stages awaits the discovery of even more pristine samples. Locally, orthopyroxene has been altered to fine anthophyllite in what is interpreted as a very late-stage reaction.

Feldspar and pyroxene megacrysts are set in a medium-grained (up to 0.5 mm) matrix of K-feldspar, quartz, plagioclase and ilmenite (Fig. 3a). In low-strain samples, these minerals are texturally immature. They tend to be blocky with a broad range of grain boundary textures. Some grains have igneous-looking, sutured boundaries but others have straight, clean 120° triple junctions (i.e. metamorphic textures). Many of the coarser feldspar crystals are cut and displaced along fractures, generally on cleavage planes, that do not extend into the matrix. K-feldspar is the most abundant matrix mineral and shows the broadest size variation, ranging from the size of matrix minerals (0.5 mm) to that of small phenocrysts (up to 2 mm). In unstrained samples, it tends to be perthitic, although the exsolution domains are rather fine-grained and inconspicuous. Locally, a subhedral to euhedral ring of spherical quartz grains (quartz drops) occurs near the rim of K-feldspar crystals. These are only present in the least deformed samples. As with the plagioclase symplectite, they are interpreted to be an igneous texture reflecting resorption during thermal fluctuations in the cooling magma.

Grain boundaries within the matrix mosaic are typically decorated with finer grains of quartz and feldspar that form a granular network throughout the samples (Fig. 3a). These fine grains are generally equant in shape and are approximately 50–100 μm in diameter. They display uniform extinction and straight equilibrium grain boundaries. They are interpreted to represent new metamorphic minerals (neocrystals) that have grown to only a limited degree within the old igneous texture (see reactions below).

In summary, the low-strain samples display a combination of igneous, metamorphic and deformational microstructures. The basic texture of large feldspar and orthopyroxene megacrysts in a medium-grained Qtz–Pl–K-feldspar–Ilm matrix is probably an original igneous characteristic. Modifications to this texture include fracturing of feldspar and orthopyroxene, limited recrystallization of original orthopyroxene and K-feldspar, overgrowths of more albitic plagioclase on igneous megacrysts, and the development of fine-grained quartz and feldspar along grain boundaries. The generally equant shape and random distribution of the new matrix minerals and plagioclase overgrowths, and the general lack of layering or foliation attest to the low level of strain in these rocks. Although undulatory extinction and bent twin planes are locally present, particularly near grain boundaries, penetrative fabrics are lacking and new metamorphic mineral growth seems to have been largely static in nature.

DEVELOPMENT OF GNEISSIC TEXTURE

The gradients in texture and fabric in the Mary granite make it ideal for investigating the transition from granite to gneiss. Although such analyses always involve the assumption that spatial variations correspond to temporal variations, the abundance of exposure and the continuous nature of the gradients on all scales increase our confidence that conclusions about the temporal evolution may be justified. Suites

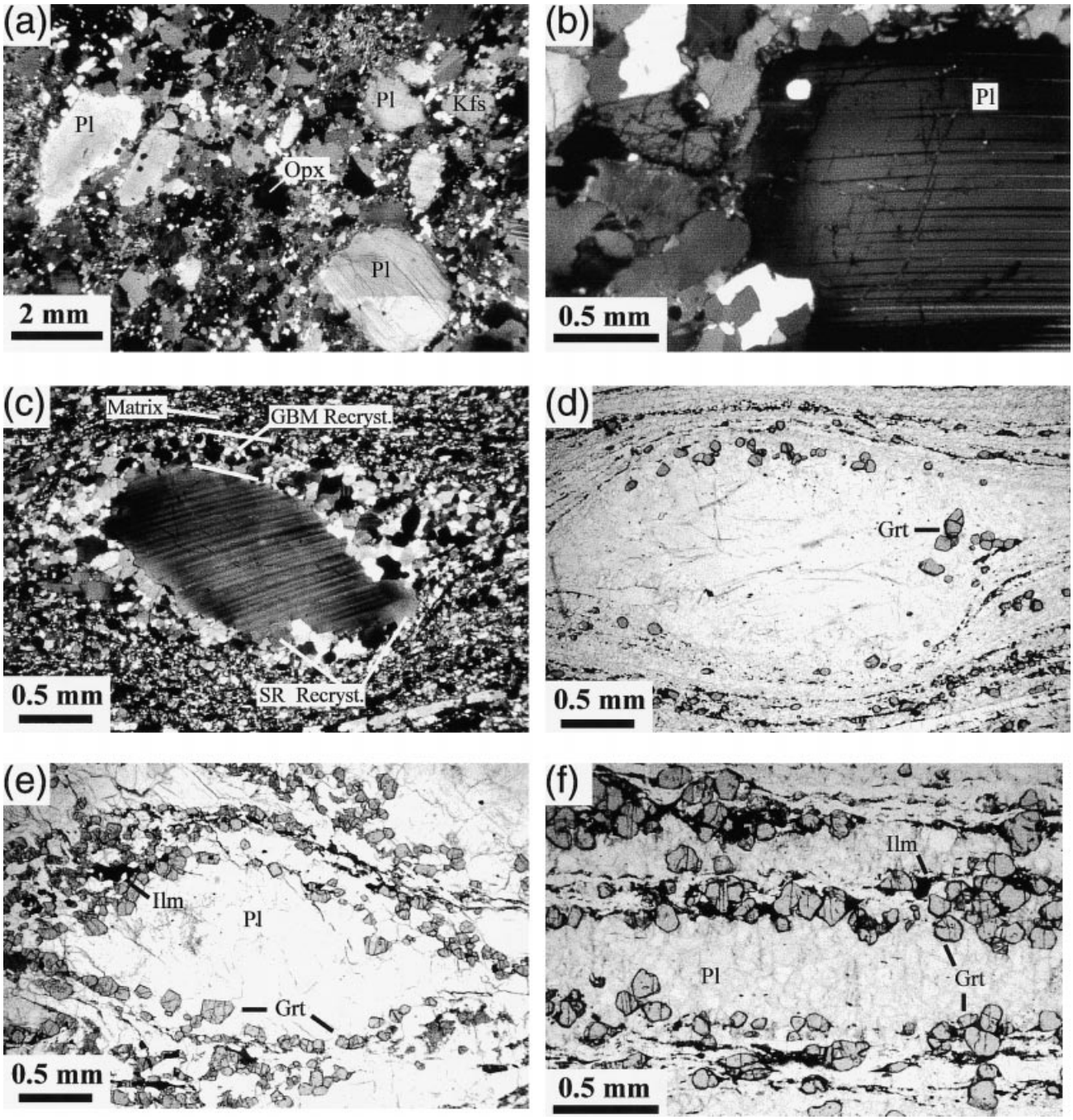

Fig. 3. Photomicrographs showing progressive deformation of plagioclase megacrysts in Mary gneiss. (a) General texture of unstrained samples. There are three general grain size classes: large plagioclase and orthopyroxene megacrysts; medium-sized grains (*c.* 1 mm in diameter), K-feldspar, plagioclase, quartz and orthopyroxene that make up the general background mosaic of low-strain samples; and fine grained (0.1–0.2 mm) quartz and feldspar along grain boundaries (these are visible as the smallest grains). (b) Plagioclase megacryst with straight twin planes and minimal undulatory extinction; edge (dark) is Na-rich metamorphic overgrowth. (c) Moderately deformed plagioclase (crossed polars) megacryst with undeformed inner core, subgrain-rich outer core, and rim of GBM recrystallized plagioclase with high-angle grain boundaries. (d) Same porphyroclast with uncrossed polars. Note small garnet crystals that have grown within the outermost GBM recrystallized plagioclase domain. (e) Moderately strained plagioclase megacryst with small low-strain core and thick recrystallized rim. Note abundant garnet within and adjacent to rim domain (see text for discussion). (f) Highly strained plagioclase megacryst (ribbon). Note abundant garnet at edge of recrystallized feldspar lithon.

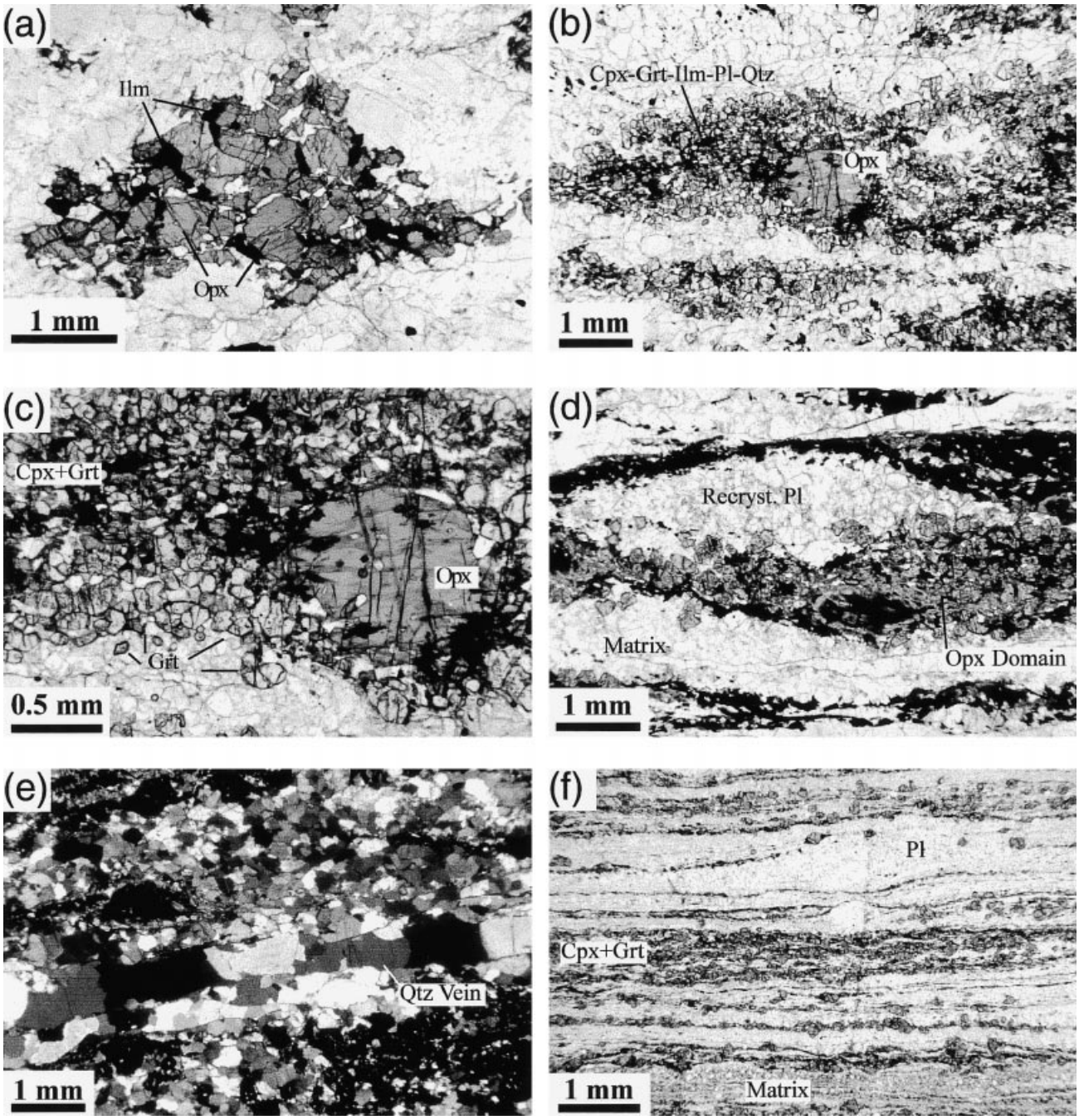

Fig. 4. Deformation of orthopyroxene megacrysts. (a) Low-strain orthopyroxene cluster with fine ilmenite. (b) Orthopyroxene megacryst with tail of fine clinopyroxene, garnet, plagioclase, ilmenite and quartz. (c) Close-up of Opx from Fig. 4(b). (d) Highly strained and neo-mineralized orthopyroxene domain and adjacent feldspar-rich and matrix domains. Note garnet crystals along the edge of Cpx–Grt–Ilm (former Opx) domains. (e) Quartz vein in recrystallized Mary granite matrix. (f) Composite view of highly strained Mary granite (gneiss) showing Grt–Cpx–Opx domains inter-layered with dynamically recrystallized plagioclase porphyroclast domains.

of samples have been collected from single outcrops with textural gradients and from the range of textures across the entire outcrop area. For the purpose of description, the samples have been divided into low-, medium-, and high-strain classes, although an essentially complete transition has been sampled in several localities (e.g. Fig. 2).

Rocks of the Mary granite show evidence for a single metamorphic reaction, synchronous with the gneiss-forming deformation. In its simplest form, the

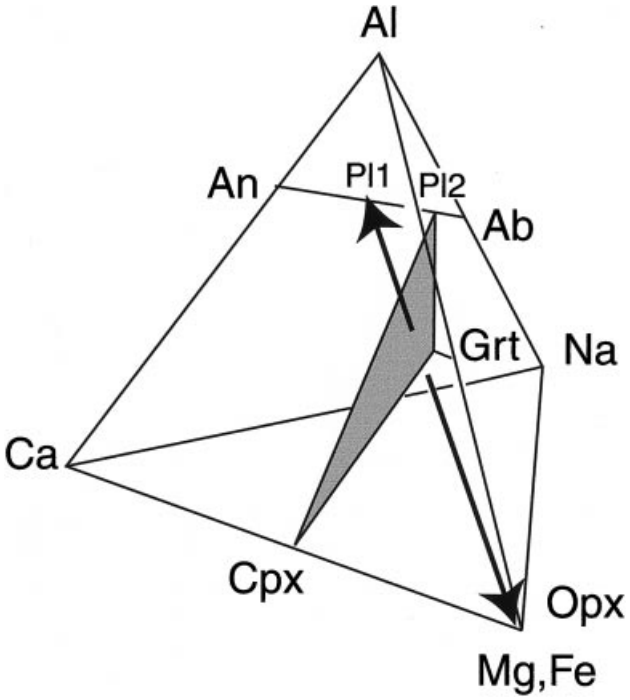

Fig. 5. A–C–F–Na phase diagram showing the generalized metamorphic reaction in hornblende-absent Mary gneiss. The phase diagram is not strictly thermodynamically valid because all compositional variation cannot be shown (Spear, 1993).

reaction involves the production of garnet, clinopyroxene, quartz and sodic plagioclase from the original orthopyroxene and more calcic plagioclase (Fig. 5). This reaction will be discussed in detail below, but is mentioned here because it plays a critical role in the textural evolution. In the following section, the development of gneissic texture will be described in the major components of the Mary granite, feldspar megacrysts, orthopyroxene megacrysts and matrix. Each seems to follow a relatively independent textural evolution during progressive deformation and metamorphism.

Evolution of feldspar megacrysts

Feldspar megacrysts in deformed Mary granite display spectacular core and mantle textures (White, 1976; Passchier & Trouw, 1996), with one main difference: garnet occurs within the outer parts of the dynamically recrystallized feldspar mantles (Fig. 3c–f). Moderately deformed plagioclase megacrysts have blocky, undeformed or weakly deformed cores with albite twinning. Locally, twin planes are bent and undulatory extinction is apparent (Fig. 3c). Outward from the cores, undulatory extinction increases, and subgrains 20–100 μm in diameter are distinguishable. The porphyroclast cores are typically surrounded by a narrow, partial to complete mantle of equant grains (20–80 μm) with a relatively consistent angular misorientation (2–5°) relative to the core. These are interpreted to be recrystallized grains developed by subgrain rotation (abbreviated SR, after Passchier & Trouw, 1996). Further outward from this mantle is a partial to complete rim of fine- to medium-grained plagioclase (50–150 μm) with variable but generally large (>10°) amounts of angular misorientation. These grains are interpreted to have developed by grain boundary migration recrystallization (abbreviated GBM, after Passchier & Trouw, 1996) in the outer, highly deformed part of the megacryst. GBM domains can be distinguished from SR domains in the composite feldspar porphyroblasts by a slightly coarser grain size, lesser degree of lattice preferred orientation, and greater angular misorientation between adjacent grains. Regions of GBM recrystallized feldspar commonly extend along the gneissic foliation defining asymmetrical dextral sigma and delta-type tails as well as symmetrical 'in-plane' tails (Hanmer & Passchier, 1991).

At higher strain, less and less of the original cores remains and the GBM recrystallized megacryst domains are increasingly elongate. At the highest strain states, feldspar megacrysts are completely recrystallized with no core remaining. They consist of lens- or rod-shaped domains of equigranular feldspar, some extending the length of a thin section or more. These can be distinguished from the matrix because they consist exclusively of equigranular plagioclase and garnet without ilmenite or quartz.

Garnet crystals are strikingly developed within the recrystallized mantles of plagioclase porphyroclasts (Fig. 3d–f). They are subhedral to euhedral, range from 30–50 μm in diameter, and occur only in the outer GBM recrystallized domains of the composite feldspar grains and in the recrystallized tails. None has been recognized within the cores or rotationally recrystallized mantles of feldspar porphyroclasts. The size of garnet crystals increases slightly and the abundance increases markedly with increasing degree of feldspar deformation. At low strain, only two or three small garnet crystals typically occur in a single plagioclase porphyroclast (Fig. 3d). At higher strain, the porphyroclasts may have a semi-continuous ring of garnet crystals in the outer portion, and larger concentrations in the tails (Fig. 3e). With progressive feldspar deformation, the garnet crystals are increasingly concentrated into layers within the plagioclase tails. This concentration seems to occur primarily by mechanical means although new garnet growth is also likely. At highest strain, narrow garnet-rich layers occur within layers of recrystallized plagioclase (Fig. 3f).

At relatively high strain, garnet crystals are also developed at the margins of porphyroclasts and ribbons. This leads to a layered package with outer garnet-rich layers, inner plagioclase-rich layers, and a central garnet-rich layer that represents the mantle-hosted garnet. The garnet- and plagioclase-rich layering, broadly corresponding to deformed plagioclase porphyroclasts, forms a major component of the gneissic layering characteristic of most Mary granite exposures.

Evolution of orthopyroxene domains

Orthopyroxene megacrysts in the Mary granite are partly replaced by garnet and clinopyroxene (±hornblende and ilmenite) (Fig. 4). In relatively low-strain samples, orthopyroxene crystals have rims of clinopyroxene, garnet and ilmenite (Fig. 4b,c). Concentrations of the new phases occur in tails or shadows adjacent to the orthopyroxene crystals and extend along the foliation. With increasing strain, as indicated by the degree of feldspar and matrix recrystallization, the orthopyroxene porphyroclasts are smaller and the Cpx–Grt–Ilm domains are larger and more concentrated into layers. In addition, some orthopyroxene crystals are fractured, generally on crystallographic cleavage planes, and dispersed along the foliation. At the highest strain, elongate regular layers of garnet, clinopyroxene and ilmenite occur with little or no orthopyroxene (Fig. 4d). A layer of slightly larger garnet crystals occurs at the edges of these Grt–Cpx–Ilm layers where they are in contact with matrix or with recrystallized plagioclase. Typically, the end product of the syntectonic orthopyroxene reaction/recrystallization is a three-layer package with a thick inner Cpx–Grt–Ilm layer bounded by thinner marginal garnet-rich layers.

Many Grt–Cpx layers (formerly orthopyroxene megacrysts) also contain hornblende. From sample to sample, the modal abundance varies from $<1\%$ (several small crystals per thin section) to $>10\%$. Hornblende abundance is generally antithetic to that of clinopyroxene. The hornblende crystals tend to be aligned with the gneissic layering. It is not clear in all cases whether hornblende was produced from clinopyroxene or if hornblende was produced with garnet during orthopyroxene breakdown. The presence of hornblende rims on some clinopyroxene suggests that at least some clinopyroxene has been subsequently converted to hornblende. Regardless of the timing, thermobarometric data suggest that hornblende grew under approximately the same metamorphic conditions as clinopyroxene, and both minerals are syntectonic with respect to the development of gneissic layering. The presence or absence of hornblende probably reflects the presence and heterogeneous distribution of H_2O in the deforming granite.

Matrix evolution

The fine-grained quartz and plagioclase that occur along grain boundaries in the least deformed samples are not present in moderately or highly deformed samples. If these grains were ever present in the more highly deformed rocks, they have coarsened so as to be indistinguishable from the other matrix minerals. Alternatively, they may have developed exclusively in undeformed rocks. They may represent new grains associated with essentially static metamorphism of the weakly deformed igneous rocks (see reactions below). Some of the new grains may also reflect local dynamic recrystallization along grain boundaries where stresses and fluids may have been concentrated.

At moderately low strain, matrix quartz grains commonly display a distinct shape preferred orientation (SPO) parallel or slightly oblique to the foliation. Some matrix feldspar grains show undulatory extinction and others are fractured and offset along crystallographic cleavage. In some moderately strained rocks, quartz ribbons with aspect ratios of 4:1 or 5:1 are present. The ribbons are generally recrystallized to equant 30–50 μm diameter grains, but the ribbon geometry is still easily recognizable. Some ribbons are parallel to the gneissic layering and others are oblique to it, defining an S-C fabric. Where present, this S-C fabric consistently indicates a dextral shear sense. At highest strains, the matrix displays a more homogenous equilibrium texture; quartz and feldspar occur as fine-grained (30–100 μm) equant crystals and only remnants of the ribbons or SPO are apparent. Grain boundaries range from straight to irregular. We interpret the quartz ribbons and SPO to be transient features involved with the transformation from the original igneous to the dynamically recrystallized texture. Once established, the equigranular recrystallized matrix fabric may be relatively strain-insensitive. Some component of post-deformational annealing may also contribute to the equant, equigranular character of matrix of the high-strain samples.

Several additional fabric elements also contribute to gneissic layering. First, many moderate and strongly layered samples contain narrow mono-mineralic layers of recrystallized quartz (Fig. 4e). Individual quartz grains are equant and generally extend completely across the width (100–200 μm) of the quartz layer. The quartz is relatively strain-free with few subgrains and only local undulatory extinction. The layers are parallel-sided and can cross an entire thin section. Layer boundaries commonly step left or right in parallel, and some fork, pinch out or overlap other layers in an en echelon fashion. These observations suggest that the layers originated as veins and were subsequently deformed and recrystallized (MacKinnon *et al.*, 1997). Thus, in addition to deformation and metamorphism of original igneous components, some compositional layering was also developed by injection of materials into the deforming rocks. It is interesting to note the presence of brittle fracturing and vein-filling (hydrothermal?) processes even at granulite facies conditions.

Some samples have narrow (mm to cm in thickness), strongly mylonitic layers. These are characterized by extremely fine matrix grain sizes (5–20 μm) and intense internal layering. Many show S-C and C′ foliations (Berthé *et al.*, 1979; Passchier & Trouw, 1996) (Fig. 4e). Rounded feldspar porphyroclasts are generally present within the mylonitic matrix. Strain was apparently partitioned into the matrix of these layers, maintaining the porphyroclasts in a relatively low strain state. The

ultramylonitic matrix contains narrow stringers of garnet and clinopyroxene, with or without hornblende and without orthopyroxene. Unlike the feldspar porphyroclasts, orthopyroxene (assumed to have originally been present) was apparently deformed and removed by reaction in these layers. Gradients between high- and low-strain domains occur on all scales. Regional (km-scale) gradients have been mapped in several areas (i.e. the Hawkes Lake area, Fig. 2), but dramatic gradients are also apparent on the thin-section or hand-specimen scale. At this scale, the gradients themselves contribute to the overall gneissic character of the rocks.

PETROLOGICAL RELATIONSHIPS

Mineral compositions

Representative mineral compositions in low-, medium- and high-strain samples are summarized in Table 2. Minerals were analysed on a Cameca SX-50 electron microprobe at the University of Massachusetts. High-resolution compositional maps were generated for most phases in order to evaluate compositional zonation. Compositional maps were also useful for showing the texture and distribution of the various feldspars because K-feldspar and plagioclase are difficult to distinguish optically. Based on the compositional maps, spot analyses and quantitative traverses were carried out. In general, compositional relationships are consistent across much of the Mary granite although absolute compositions do vary slightly from sample to sample. These variations probably represent primary compositional variation between the different bodies of Mary granite, as also indicated by whole-rock compositions.

Plagioclase megacrysts have two compositions, represented by core and rim. Core compositions are invariably richer in anorthite than rims (Fig. 6). The compositional core–rim boundaries are relatively sharp and typically occur between the SR recrystallized and GBM recrystallized domains of the deformed feldspar. Core compositions range from An_{47} to An_{40}, although values as low as An_{35} occur in one sample (S809B). Recrystallized plagioclase has a composition of approximately An_{22} and is similar in composition throughout any one sample, including GBM recrystallized rims of plagioclase porphyroclasts, porphyroclast tails and matrix plagioclase. Some cores are slightly zoned with decreasing anorthite component toward the rim. For example, sample S825B (Table 2) shows continuous zoning from An_{47} to An_{40} before a sharp drop to An_{21} in the recrystallized rim. This zoning is interpreted to be of igneous origin because it exclusively occurs within the core region. Significant diffusional exchange of Na and Ca, involving coupled substitution with Al and Si, would be extremely slow in these large crystals (Grove *et al.*, 1984).

K-feldspar is also characterized by two compositions, corresponding to megacrysts and recrystallized matrix grains. Megacrysts are strongly perthitic. Exsolution lamellae of albite are closely spaced and narrow (2–10 μm), making it impossible to analyse the exsolved components separately. Compositions, determined by averaging 50 or more broad-beam analyses from traverses across exsolved crystals, are similar from sample to sample (Kfs_{78}, Ab_{20}, An_{02}). Matrix K-feldspar and edges of some megacrysts are generally non-perthitic. Most are approximately $Kfs_{87–90}$, $Ab_{09–11}$, $An_{0.00–0.01}$. The perthitic, Na-rich, K-feldspar megacrysts are interpreted on both textural and compositional grounds to be relict igneous minerals. Rim and matrix K-feldspar compositions are interpreted to be metamorphic. Some K–Na diffusion may have also occurred at the edges of K-feldspar crystals as indicated by the lack of exsolution lamellae near the edges of some megacrysts.

Orthopyroxene (ferrosilite) is generally unzoned, and compositions are uniform on the thin-section scale. From sample to sample, Mg numbers (Mg/Mg + Fe) range from 0.12 to 0.30, apparently reflecting variations in the original bulk composition. No regular relationship has been observed between the Mg number and the degree of deformation or reaction; distribution coefficients with other ferromagnesian phases are similar from sample to sample, and thermobarometric calculations suggest that orthopyroxene was in equilibrium with garnet and clinopyroxene under metamorphic conditions (see below). Because orthopyroxene is believed to have been of igneous origin, diffusion or recrystallization must have occurred in order to maintain equilibrium during metamorphism. Clinopyroxene (augite) is also relatively uniform in composition, with Mg numbers near 0.5. Individual crystals have unzoned interiors with a sharp increase in Mg/Mg + Fe near the rims. This rim zoning is heterogeneously developed and is most pronounced near garnet-rich domains, apparently reflecting diffusional exchange with garnet during cooling.

Garnet is grossular-rich almandine (*c.* Alm_{70}, $Gros_{20}$, $Prp_{5–10}$). Garnet cores are unzoned, and are interpreted to represent peak metamorphic compositions. Rims typically display increasing X_{Fe} and decreasing X_{Mg}, interpreted to represent diffusional re-equilibration during cooling. As discussed below, the fact that these rims are not only developed adjacent to ferromagnesian minerals but also against other minerals indicates the presence of at least some grain boundary fluid during metamorphism. X_{Ca} is nearly constant from core to rim. Garnet compositions are identical in the two main textural settings (i.e. completely enclosed within recrystallized plagioclase, or associated with orthopyroxene). Most amphibole is hornblende according to the classification of Giret *et al.* (1980). Ilmenite is the only other ferromagnesian phase in the Mary granite. It has a nearly end-member composition, and no variation was seen between compositions of large, texturally early ilmenite and fine late-stage ilmenite.

Table 2. Mineral compositions from selected samples of Mary granite*.

	Undeformed S823B			Intermediate strain S831					S809B					Highly strained S-513						
	Opx	Pl (core)	Pl (rim)	Kfs (matrix)	Grt2	Opx	Pl (core)	Pl (rim)	Hbl	Grt	Pl (core)	Pl (rim)	Hbl	Opx	Grt	Opx	Cpx	Pl (core)	Pl (rim)	Hbl
SiO_2	47.90	56.12	61.72	65.03	36.69	47.73	59.38	63.46	39.68	37.22	58.29	63.89	40.56	47.84	37.01	49.34	50.01	57.36	60.57	40.90
TiO_2	0.09	na	na	0.03	0.00	0.05	na	na	2.03	0.06	na	na	1.29	0.12	0.02	0.07	0.15	na	na	2.24
Al_2O_3	0.86	28.12	24.72	18.52	20.68	0.32	26.21	23.53	10.64	20.25	26.94	23.64	10.86	0.53	20.91	0.95	2.06	26.84	24.63	11.43
FeO	43.49	0.05	0.08	0.27	32.11	42.93	0.06	0.15	24.55	31.98	0.01	0.00	22.94	41.24	30.60	34.88	15.55	0.08	0.31	21.46
MnO	0.82	na	na	na	0.72	0.30	na	na	0.05	0.62	na	na	0.07	0.35	0.66	0.34	0.09	na	na	0.08
MgO	6.25	na	na	na	1.72	8.07	na	na	6.03	1.75	na	na	5.43	8.42	2.96	12.90	9.76	na	na	7.81
CaO	0.88	10.16	5.93	0.38	6.97	0.69	7.88	4.79	11.04	7.02	8.45	4.58	10.92	1.03	6.96	0.73	21.24	8.55	5.88	10.93
Na_2O	0.02	6.10	8.64	2.23	na	na	6.93	8.99	1.57	na	6.98	9.30	1.55	0.03	0.02	0.03	0.61	6.69	8.46	1.66
K_2O	na	0.15	0.15	12.94	na	na	0.18	0.12	1.76	na	0.17	0.20	1.61	na	na	na	na	0.19	0.11	1.73
Σ	100.30	100.74	101.25	99.83	98.89	100.09	100.64	101.03	97.35	98.93	100.84	101.60	95.24	99.55	99.13	99.23	99.48	99.72	99.95	98.23
Cations																				
Si	1.99	2.51	2.71	2.99	2.99	1.97	2.63	2.78	6.28	3.02	2.59	2.78	6.49	1.98	2.98	1.97	1.92	2.58	2.70	6.29
Ti	0.00	0.00	0.00	0.00	0.00	0.00	0.00	0.00	0.24	0.00	0.00	0.00	0.16	0.00	0.00	0.00	0.00	0.00	0.00	0.26
Al	0.04	1.48	1.28	1.00	1.98	0.02	1.37	1.22	1.99	1.93	1.41	1.21	2.05	0.03	1.98	0.04	0.09	1.42	1.29	2.07
Fe	1.51	0.00	0.00	0.01	2.19	1.49	0.00	0.01	3.25	2.11	0.00	0.00	3.07	1.42	2.06	1.17	0.50	0.00	0.01	2.76
Mn	0.03	–	–	–	0.05	0.01	–	–	0.01	0.04	–	–	0.01	0.01	0.04	0.01	0.00	–	–	0.01
Mg	0.39	–	–	–	0.21	0.50	–	–	1.42	0.21	–	–	1.30	0.52	0.36	0.77	0.56	–	–	1.79
Ca	0.04	0.49	0.28	0.02	0.61	0.03	0.37	0.22	1.87	0.61	0.40	0.21	1.87	0.05	0.60	0.03	0.87	0.41	0.28	1.80
Na	0.00	0.53	0.74	0.20	–	–	0.60	0.76	0.48	–	0.60	0.79	0.48	0.00	0.00	0.00	0.05	0.58	0.73	0.49
K	–	0.01	0.01	0.76	–	–	0.01	0.01	0.36	–	0.01	0.01	0.33	–	–	–	–	0.01	0.01	0.34
X_{Mg}	0.20				0.09	0.25	0.30	0.09			0.30	0.27	0.15	0.40	0.53			0.39		
En/Di	0.20					0.25					0.26		0.39	0.28						
Fs/Hd	0.77					0.73					0.71		0.59	0.25						
Wo	0.02					0.02					0.02		0.02	0.44						
An		0.47	0.27	0.02			0.38	0.23		0.40	0.21						0.41	0.28		
Ab		0.52	0.72	0.20			0.61	0.77		0.59	0.78						0.58	0.72		
Kfs		0.01	0.01	0.78			0.01	0.01		0.01	0.01						0.01	0.01		
Prp					0.07	0.07					0.12									
Sps					0.02	0.01					0.01									
Grs					0.20	0.21					0.20									
Alm					0.72	0.71					0.67									

* Complete data set available from mlw@geo.umass.edu; na, not analysed; $X_{Mg} = Mg/(Mg + Fe)$.

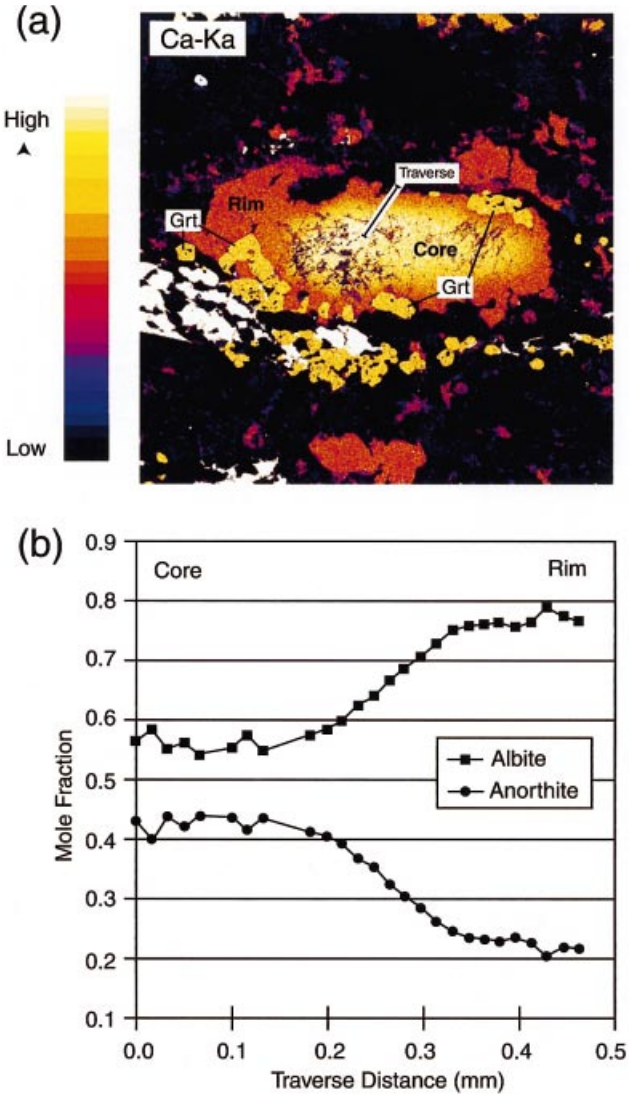

Fig. 6. (a) Ca Kα wavelength dispersive X-ray map of a moderately deformed plagioclase megacryst. Red–orange rim represents GBM recrystallized plagioclase with more Ab-rich composition. Equant yellow areas are garnet crystals in recrystallized rim. Yellow–orange region in centre of plagioclase is An-richer (igneous) core. (b) Core-to-rim compositional traverse of plagioclase megacryst from Fig. 6(a).

Phase relationships and thermobarometry

Peak metamorphic conditions for the Mary granite have been estimated using numerous equilibria and two different methods, internally consistent thermobarometry and calibrated thermobarometry. Grt–Px–Pl assemblages were characterized using the internally consistent database and software (TWQ version 2.02) of Berman (1991, 1992). However, instead of plotting all dependent and independent equilibria, we have chosen to plot only an independent set of reactions. In choosing the independent set, we have attempted to select at least one temperature-sensitive and one pressure-sensitive reaction, and if possible, we have used reactions that have also been calibrated as thermometers or barometers (i.e the garnet–clinopyroxene thermometer or garnet–clinopyroxene–plagioclase–quartz barometer). Many workers still have great confidence in calibrated thermobarometers. The use of well-known reactions allows comparison between mixing models, datasets and alternative calibrations (Fig. 7).

For hornblende-bearing assemblages, we have used both calibrated and internally consistent database thermobarometry. Attempts to constrain hornblende-bearing equilibria using the dataset of Berman (version 1.02; Berman, 1991, 1992; Mader *et al.*, 1994) have yielded mixed results. Data for many samples are essentially identical to pyroxene-based calculations (Fig. 7). However, other samples produce unreasonable results when compared to pyroxene-based equilibria or to calibrated equilibria. In all of these cases, the barometer reactions suggested by Mader *et al.* (1994) are consistent with other equilibria, but thermometer reactions, based on Fe–Mg exchange, are inconsistent. High or low temperature estimates lead to high or low intersections with barometer reactions, and thus anomalous *P–T* estimates when used alone. We suspect that the anomalous temperatures result from late Fe–Mg diffusional exchange in hornblende, and perhaps from problems resulting from ferric iron in hornblende. The calibrated Hbl–Pl thermometer of Holland & Blundy (1994), based on Na–Ca partitioning between hornblende and quartz, seems to be less susceptible to late-stage resetting and is less dependent on ferric/ferrous ratios. Therefore, we generally included this thermometer with the otherwise internally consistent equilibria for hornblende-bearing rocks, especially for those without other *P–T* constraints.

Compositional X-ray maps were collected from all samples to be used for thermobarometry, including maps of all porphyroblasts and of matrix domains, in order to evaluate zoning within minerals and compositional variation between metamorphic or structural domains. For peak metamorphic conditions, core compositions of garnet, pyroxene and hornblende were generally used because all of these phases show some amount of diffusional re-equilibration near the rims. Plagioclase compositions were taken from dynamically recrystallized mantles because cores are interpreted to retain igneous compositions (see below). The careful selection of compositions based on high-resolution compositional mapping and microstructural analysis may be an important factor leading to the consistency of the diverse equilibria (Fig. 7) and the sample-to-sample consistency observed throughout the Mary granite (Fig. 8).

Metamorphic conditions

Temperature estimates from metamorphic minerals, regardless of the intensity of deformational fabrics, range from 700–800 °C and pressures range from 0.9–1.1 GPa (Fig. 8). The general consistency of Opx- and Cpx-based estimates indicates that the fragmented

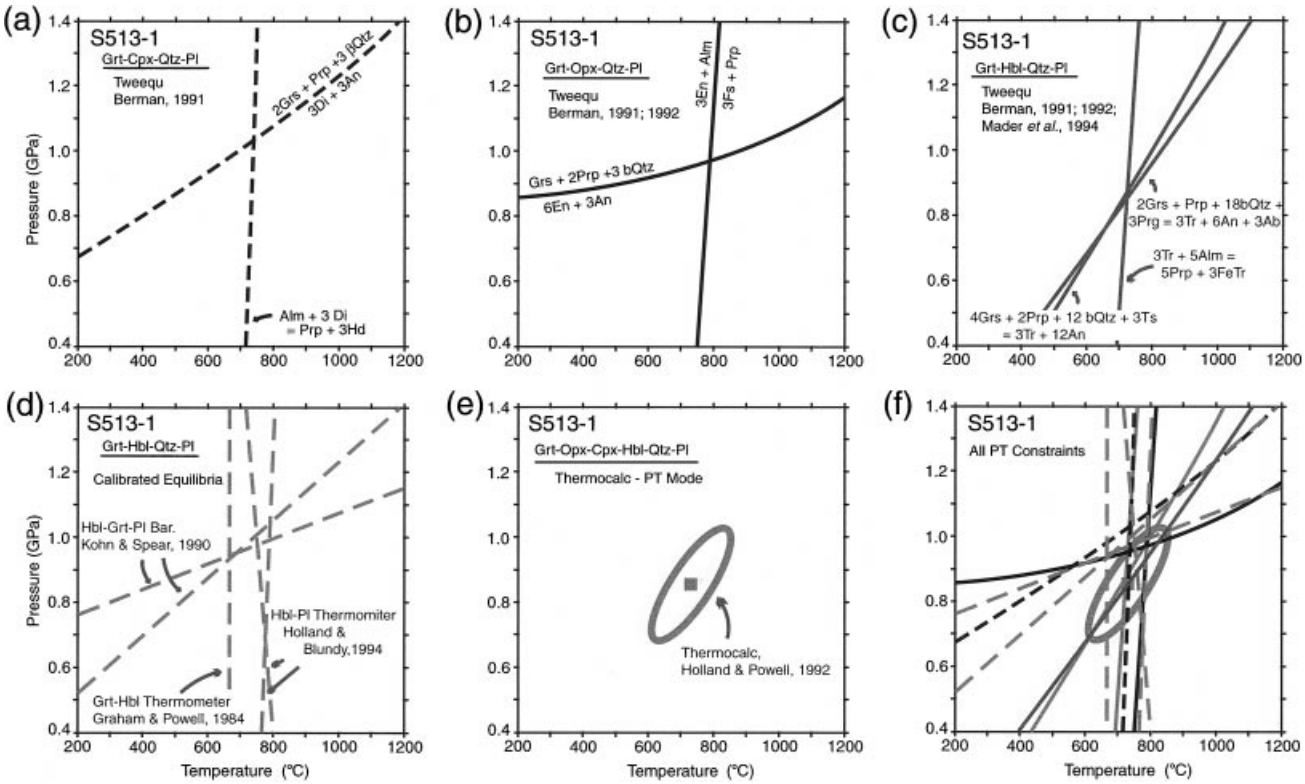

Fig. 7. Comparison of methods for *P–T* estimation in the Mary granite. Bold lines (a,b) represent internally consistent thermobarometry using TWQ software (Berman, 1991) and thermodynamic database of Berman (1992). Hornblende-bearing equilibria use thermodynamic data and follow recommendations of Mader *et al.* (1994). Solid bold lines (b) are Grt–Opx–Pl equilibria; dashed bold lines (a) are Grt–Cpx–Pl equilibria. Grey lines (c,d) are calibrated thermobarometers (equilibria labelled on plot). (e) Estimated metamorphic conditions and 95% confidence ellipse based on THERMOCALC software (Powell & Holland, 1988) in average *P–T* mode and the database of Holland & Powell (1998). (f) Comparison of all methods showing consistency of internally consistent and calibrated equilibria. This consistency is critical for comparing Mary granite samples with distinct metamorphic assemblages.

and irregular orthopyroxene have maintained equilibrium with the product Grt–Aug–Pl–Hbl assemblages. Moreover, estimates based on hornblende-bearing equilibria are consistent with the hornblende-absent assemblages. This indicates that hornblende is not a late-stage retrograde phase, but instead is a peak (or near-peak) metamorphic phase. Hornblende is apparently a stable phase in the product assemblage where sufficient water is present; augite occurs in water-poor or water-absent assemblages.

Igneous crystallization conditions

Field and thin-section textures indicate that the Mary granite was emplaced at depths corresponding to the recorded metamorphic pressures (1.0 ± 0.1 GPa). This interpretation is based on the fact that the granite was intruded syntectonically during granulite facies dextral shearing (Hanmer *et al.*, 1994). There is no evidence for decompression or exhumation during the time of Mary magma emplacement or during its subsequent metamorphism.

We have attempted to constrain the crystallization temperatures using two-feldspar thermometry. Plagioclase core compositions are significantly more An-rich than recrystallized rims, and K-feldspar cores are distinctly perthitic compared with recrystallized rims. Because of the large size and unrecrystallized character of these megacrysts, and because of the slow rate of diffusion (at least that involving exchange of Na and Ca in plagioclase), we suggest that igneous compositions are preserved to some degree in these relict phases. Calculations using a range of solution models and mixing data were made using the software SOLVCALC (Wen & Nekvasil, 1994). Temperature estimates based on Ca or Na partitioning are consistently near 900 °C regardless of the solution model (Fig. 9). Estimates based on K partitioning are lower. This may reflect diffusion of K between feldspars (and hornblende?), whereas Ca diffusion did not substantially modify the igneous partitioning. Thus, we interpret the parent Mary granite magma to have been emplaced at approximately 900 °C and 0.9–1.1 GPa.

Metamorphic reactions

Figure 5 summarizes phase relationships in ACFN compositional space. This plot is not a rigorous

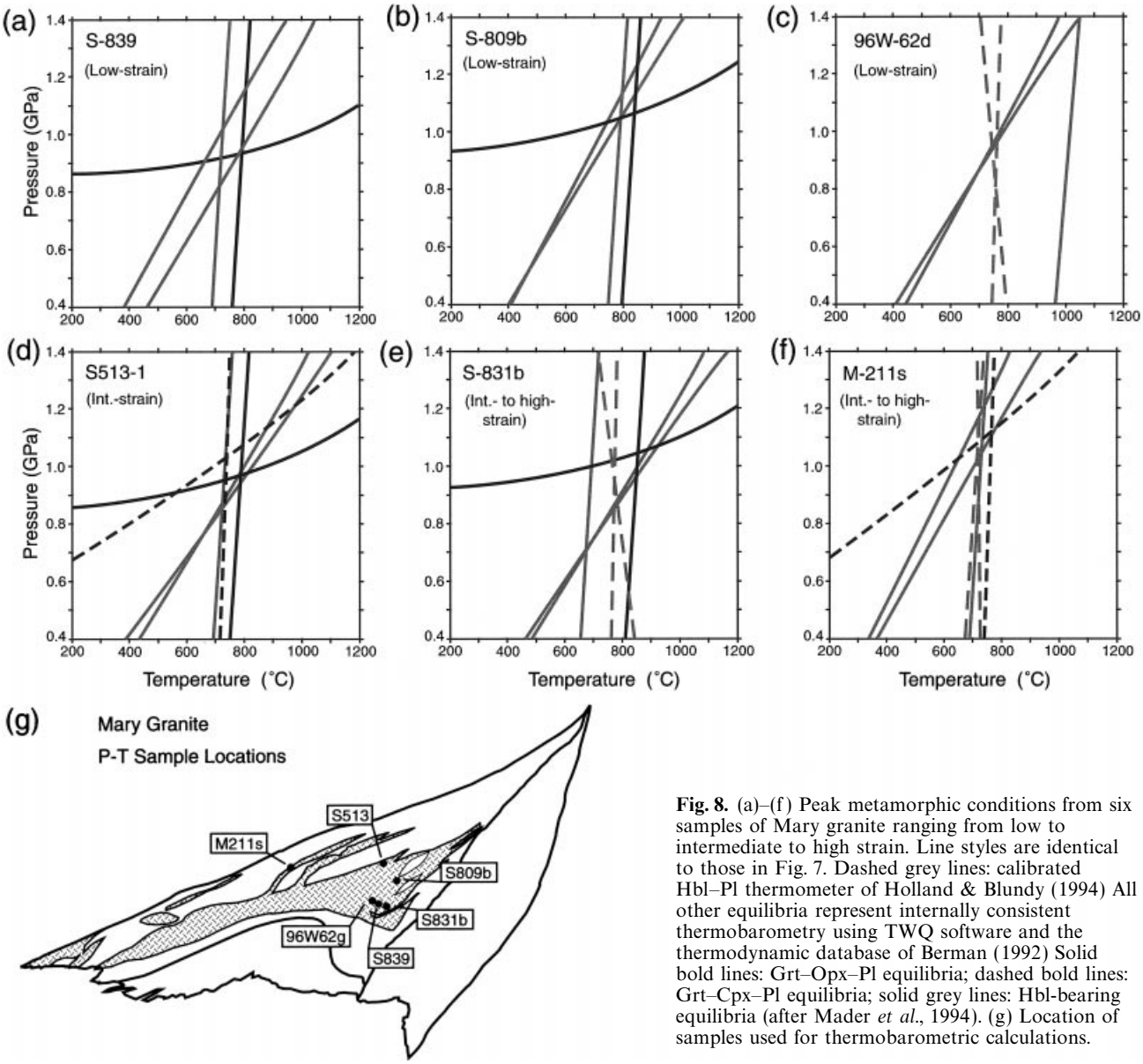

Fig. 8. (a)–(f) Peak metamorphic conditions from six samples of Mary granite ranging from low to intermediate to high strain. Line styles are identical to those in Fig. 7. Dashed grey lines: calibrated Hbl–Pl thermometer of Holland & Blundy (1994) All other equilibria represent internally consistent thermobarometry using TWQ software and the thermodynamic database of Berman (1992) Solid bold lines: Grt–Opx–Pl equilibria; dashed bold lines: Grt–Cpx–Pl equilibria; solid grey lines: Hbl-bearing equilibria (after Mader *et al.*, 1994). (g) Location of samples used for thermobarometric calculations.

thermodynamically valid phase diagram in that it cannot show all important compositional variation, but it provides a useful perspective on the possible reactions (Spear, 1993). For hornblende-absent assemblages, the ACFN reaction between the observed igneous and metamorphic minerals can be written

$$\mathrm{Opx} + \mathrm{Pl}_1 = \mathrm{Grt} + \mathrm{Cpx} + \mathrm{Pl}_2 \qquad (1)$$

where Pl_1 and Pl_2 represent the plagioclase core (Ca-richer) and rim (Ca-poorer), respectively. For the compositions of the Mary granite, this reaction can be approximately balanced as:

$$2.2\ \mathrm{Opx} + 8.0\ \mathrm{Pl}_1 = 1.25\ \mathrm{Grt} + 1\ \mathrm{Cpx} + 6.7\ \mathrm{Pl}_2 + 1.2\ \mathrm{Qtz} \qquad (2)$$

Where hornblende is present, the peak assemblage in the ACFN system becomes a four-phase volume and the reactions relating the igneous to metamorphic assemblages are:

$$\mathrm{Opx} + \mathrm{Pl}_1 = \mathrm{Grt} + \mathrm{Hbl} + \mathrm{Cpx} + \mathrm{Pl}_2 \qquad (3)$$

$$4.8\ \mathrm{Opx} + 21.6\ \mathrm{Pl}_1 + 0.8\ \mathrm{Ilm} = 1.2\ \mathrm{Grt} + 0.9\ \mathrm{Hbl} + 1.0\ \mathrm{Cpx} + 18.6\ \mathrm{Pl}_2 + 0.03\ \mathrm{Qtz} \qquad (4)$$

for the model and Mary granite systems, respectively.

Reaction (1) was investigated experimentally by Green & Ringwood (1967). It defines the boundary between the medium- and high-pressure granulite fields. The reaction is shown on Fig. 10, along with estimated igneous and metamorphic conditions for the Mary granite. The Mary granite magma apparently crystallized in the medium-pressure granulite field and

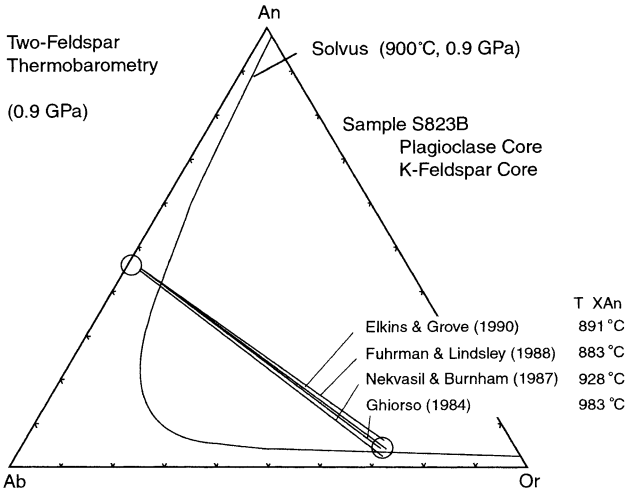

Fig. 9. Two-feldspar thermometry using interpreted igneous feldspar compositions (see text for discussion). Tie lines show three solution models for the same feldspar compositions at 0.9 GPa. Ca partitioning consistently yields 900 °C. K partitioning yields lower temperatures reflecting the K-poor nature of the plagioclase, interpreted as reflecting post-crystallization diffusion of K from plagioclase to matrix K-feldspar. Calculations and graphics were done using the SOLVCALC software (Wen & Nekvasil, 1994).

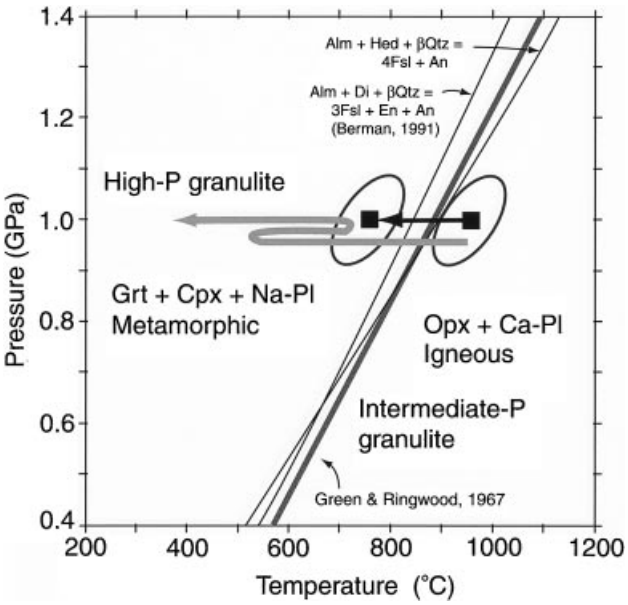

Fig. 10. Simplified phase diagram showing inferred metamorphic reaction and calculated igneous and metamorphic conditions for Mary granite. Shaded reaction curve is from Green & Ringwood (1967). Solid reactions were calculated with the database of Berman (1992) and composition from Table 2 (sample S513). The *P–T* path may involve simple cooling (solid path) from igneous conditions or cooling with subsequent reheating (grey path) perhaps due to later phases of the Mary granite.

then cooled into the high-pressure granulite field, where deformation and metamorphism occurred to different degrees.

DISCUSSION

The development of compositional layering in the Mary granite involves a progressive, complementary interaction between metamorphism and deformation in three microdomains, corresponding to plagioclase phenocrysts, orthopyroxene phenocrysts and matrix in the undeformed igneous rocks (Fig. 11). Plagioclase phenocrysts were strained and dynamically recrystallized forming core and mantle structures. Garnet grew syntectonically in the recrystallized plagioclase mantles. The recrystallized plagioclase and the new garnet grains were drawn out into layers, and additional garnet developed along the edges of the plagioclase-rich laminae. Orthopyroxene crystals were progressively replaced by clinopyroxene and garnet (and hornblende if sufficient water was present). These products were dispersed into layers along with fragments of the original orthopyroxene megacrysts. The igneous matrix underwent progressive reaction and dynamic recrystallization, passing through fabric stages involving S-C fabrics, S-C-C′ fabrics, with local ultramylonitic domains. Although transient, these composite fabrics contribute to the overall gneissic layering in most outcrops. An additional component of the gneissic layering involves quartz veins syntectonically emplaced into the developing gneiss.

The degree of metamorphic reaction in the Mary granite can be qualitatively correlated with the intensity of deformation. This suggests that deformation is an important kinetic factor in the metamorphism of these high-grade, relatively dry rocks. The history shown on Fig. 10 is an example of reaction understepping, in that the high-temperature assemblages may have cooled to the low-temperature side of the reaction, but they were sluggish to re-equilibrate without deformation. This explains the co-existence of igneous assemblages in low-strain rocks and metamorphic assemblages in higher-strain rocks. The metamorphic assemblages may have developed simply due to dynamic recrystallization along the cooling path, but it seems equally likely that they developed during subsequent periods of reheating (shaded path on Fig. 10), perhaps associated with the intrusion of later pulses of the Mary granite.

Both brittle and ductile deformation processes were locally active in the fabric transition. Although dislocation creep (accommodated by dynamic recrystallization) of quartz and feldspar was the dominant strain mechanism, fracturing of feldspar and particularly of Opx on cleavage planes may have also played a role in exposing new reactant surfaces and in contributing to the overall layered character of the rocks (i.e. by dispersing fragments into layers). In addition, quartz veins seem to be a locally important component of the gneissic fabric. Because the veins (and the vein quartz) show evidence for different degrees of deformation and truncation of fabric, the fractures are interpreted to

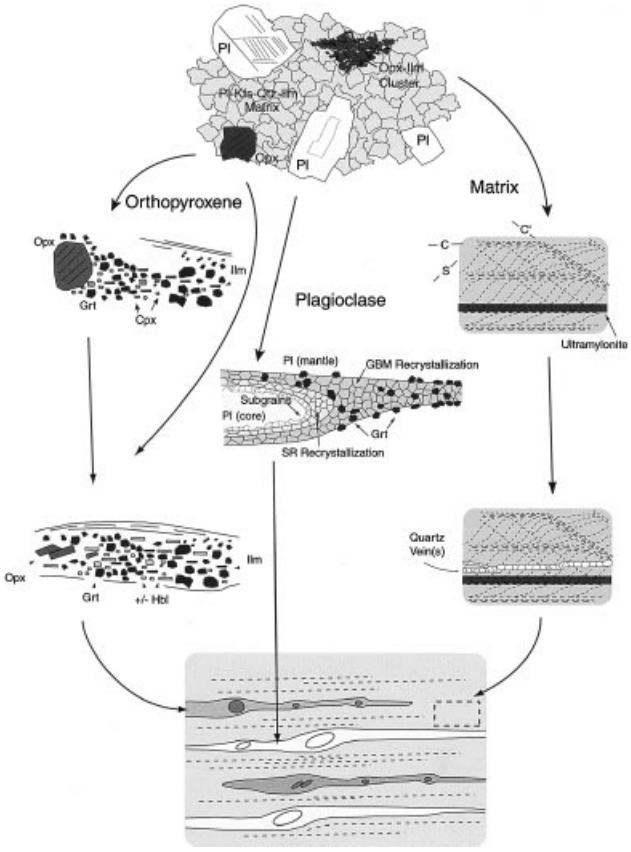

Fig. 11. Schematic diagram showing the development of gneissic fabric in Mary granite (gneiss). The gneissic fabric reflects the combined evolution of three fabric domains: feldspar megacrysts, orthopyroxene megacrysts and matrix domains. See text for discussion.

have formed during the overall granulite facies flow, and thus represent local brittle behaviour within the ductilely deforming rock. This may reflect locally high fluid pressures (although no direct correlation has been noted with the abundance of hydrous minerals such as hornblende) or locally high strain rate domains within the heterogeneously straining rock.

Although deformation was apparently critical for significant progress of metamorphic reactions, the metamorphic reactions and partial reactions may themselves have influenced the progress and localization of deformation. Metamorphism contributed to a reduction in grain size by replacing large plagioclase and orthopyroxene megacrysts by finer clinopyroxene, garnet and Na-rich plagioclase. Also, although the driving energy for dynamic recrystallization was certainly dislocation-related (i.e. strain-related), a component of the driving force for neo-mineralization and grain growth must have also involved the chemical disequilibrium of the relict igneous assemblage.

One of the most striking observations concerning the metamorphic reaction and fabric transition is that garnet and clinopyroxene developed in distinctly different settings; clinopyroxene grew adjacent to orthopyroxene while garnet grew predominantly within, and at the margins of, plagioclase mantles. Apparently, orthopyroxene formed a favourable environment for clinopyroxene nucleation and growth. This probably reflects the similarity in crystal structure of the two phases. In contrast, the localization of garnet in plagioclase mantles may reflect a tendency for garnet to develop in Al-rich domains. We suggest that the mobility of aluminium was a limiting factor in these rocks. Fe and Mg were able to diffuse, perhaps in a grain boundary fluid, into the recrystallizing plagioclase mantles, allowing equilibrium almandine garnet to grow. The recrystallization is critical for the diffusion process because no garnet has been noted in the undeformed plagioclase cores. We nonetheless find it surprising that garnet crystals nucleate within and not merely adjacent to the plagioclase mantles. Apparently some structural or chemical characteristic of the dynamically recrystallizing plagioclase is particularly favourable for garnet nucleation.

Compositional segregation is distinctly less apparent in samples richest in hornblende. Domains corresponding to plagioclase and orthopyroxene megacrysts can still be recognized, but they occur in a more homogenous Hbl–Pl–Qtz matrix. Diffusion may be faster in these more hydrous domains, and thus reaction products may be less restricted to particular settings. This may point to an additional link between gneissic fabrics and relatively dry metamorphic conditions.

One important implication of this work is that it is possible to recognize the three basic components of the original igneous rocks even in highly deformed samples. Domains corresponding to recrystallized plagioclase, reacted and deformed orthopyroxene, and original matrix are distinguishable in most rocks, as are recrystallized quartz veins (Fig. 11). Although recognizable, the relative volumes and compositions of the various domains have been modified significantly, and several original domains have merged into nearly continuous layers. Thus, it is generally not possible to estimate the magnitude of finite strain based on the deformed shape of the originally igneous domains, but it is clear that the basic location and distribution of gneissic layers were inherited from the igneous texture.

TECTONIC IMPLICATIONS

The deformation and metamorphic model for the evolution of the Mary granite has implications for the history of the EAmt in general. The (2.6 Ga) Mary granite was emplaced syntectonically. The rocks were metamorphosed and deformed during near isobaric cooling. As noted, there is no evidence for decompression or exhumation during the period of emplacement or metamorphism of the Mary rocks. This is consistent with other results from the EAmt which indicate that the rocks were deformed during strike–slip ductile shearing but were not uplifted or exhumed

during the shearing event (Hanmer *et al*., 1994; Kopf *et al*., 1997).

We visualize the crust as being in near-isostatic equilibrium during the time of Mary granite emplacement and deformation. The deformational event was certainly regional in nature, but it may have been localized in this particular domain during the thermal disequilibrium resulting from the granite emplacement itself. That is, the syntectonic metamorphism may represent cooling from igneous temperatures to ambient regional metamorphic temperatures. The P–T path for the Mary granite is characterized by near-isobaric cooling; the prograde part of the path is not apparent because the granite was emplaced at maximum metamorphic pressures (i.e. 1.0 GPa). We interpret the Mary granite to preserve aspects of the behaviour of the deep crust during strike–slip shearing of an isobarically stable crust (i.e. of rocks that may have resided in the deep crust for a period of time) rather than during a short-lived time of crustal thickening. As such, the rocks may provide a glimpse of the character and behaviour of other relatively stable deep crustal regions that presently can be characterized only by seismic signature.

ACKNOWLEDGEMENTS

This research was partially supported by National Science Foundation Grant NSF-EAR-9406443 to M.L.W. The authors sincerely thank J. Tullis, J. McLelland and R. Berman for their careful reviews of this manuscript. The manuscript was significantly improved because of their comments and several serious mistakes were avoided. We also thank S. Seaman, M. Jercinovic and D. Snoeyenbos for comments, general discussions and technical help with XRF and electron probe analyses. This is Geological Survey of Canada publication number 1999055.

REFERENCES

Berman, R. G., 1991. Thermobarometry using multi-equilibrium calculations: a new technique, with petrological applications. *Canadian Mineralogist*, **29,** 833–855.

Berman, R. G., 1992. Thermobarometry with estimation of equilibration state (TWEEQU): an IBM-compatible software package. *Geological Survey of Canada Open File* 2534.

Berthé, D., Choukroune, P. & Jegouzo, P., 1979. Orthogneiss, mylonite and noncoaxial deformation of granites: the example of the South Armorican Shear Zone. *Journal of Structural Geology*, **1,** 31–42.

Bowes, D. R. & Park, R. G., 1966. Metamorphic segregation banding in the Loch Kerry Bastie sheet from the Lewisian of Gairloch, Ross-shire Scotland. *Journal of Petrology*, **7,** 306–330.

Davidson, A., 1984. Identification of ductile shear zones in the southwestern Grenville Province of the Canadian Shield. In: *Precambrian Tectonics Illustrated* (eds Kroner, A. & Greiling, R.), pp. 207–235. E. Schweitz Verlag, Stuttgart.

Elkins, L. T. & Grove, T. L., 1990. Ternary feldspar experiments and thermodynamic models. *American Mineralogist*, **75,** 544–559.

Fuhrman, M. L. & Lindsley, D. H., 1988. Ternary-feldspar modeling and thermometry. *American Mineralogist*, **73,** 201–215.

Ghiorso, M. S., 1984. Activity/composition relations in the ternary feldspars. *Contributions to Mineralogy and Petrology*, **87,** 282–296.

Giret, A., Bonin, B. & Leger, J. M., 1980. Amphibole compositional trends in oversaturated and undersaturated alkaline plutonic ring-complexes. *Canadian Mineralogist*, **18,** 481–495.

Goodacre, A. K., Grieve, R. A. F., Halpenny, J. F. & Sharpton, V. L., 1987. Horizontal gradient of the Bouguer gravity anomaly map of Canada. *Geological Survey of Canada, Canadian Geophysical Atlas, Map 5, scale 1 : 10,000,000*.

Green, D. H. & Ringwood, A. E., 1967. An experimental investigation of the gabbro to eclogite transformation and its petrological applications. *Geochimica et Cosmochimica Acta*, **31,** 767–833.

Grove, T. L., Baker, M. B. & Kinzler, R. J., 1984. Coupled CaAl–NaSi diffusion in plagioclase feldspar: experiments and applications to cooling rate speedometry. *Geochimica et Cosmochimica Acta*, **48,** 2113–2121.

Hanmer, S., 1994. Geology, East Athabasca mylonite triangle, Saskatchewan. *Geological Survey of Canada Map 1859A, scale 1 : 100,000*.

Hanmer, S. & Kopf, C., 1993. The Snowbird tectonic zone in District of Mackenzie, Northwest Territories. *Geological Survey of Canada, Current Research*, **93–1C,** 41–52.

Hanmer, S. & Passchier, C. W., 1991. Shear-sense indicators: a review. *Geological Survey of Canada Paper*, **90-17**.

Hanmer, S., Darrach, M. & Kopf, C., 1992. The East Athabasca mylonite zone: an Archean segment of the Snowbird tectonic zone in Northern Saskatchewan. *Geological Survey of Canada, Current Research*, **92–1C,** 19–29.

Hanmer, S., Kopf, C., Parrish, R. & Williams, M., 1994. Striding-Athabasca mylonite zone: I. Complex Archean deep crustal deformation in the East Athabasca Mylonite Triangle, N. Saskatchewan. *Canadian Journal of Earth Sciences*, **31,** 1287–1300.

Hanmer, S., Williams, M. & Kopf, C., 1995. Striding-Athabasca mylonite zone: implications for the Archean and Early Proterozoic tectonics of the western Canadian Shield. *Canadian Journal of Earth Sciences*, **32,** 178–196.

Hoffman, P. F., 1988. United plates of America, the birth of a craton: Early Proterozoic assembly and growth of Laurentia. *Annual Review of Earth and Planetary Sciences*, **16,** 543–603.

Holland, T. & Blundy, J., 1994. Non–ideal interactions in calcic amphiboles and their bearing on amphibole-plagioclase thermometry. *Contributions to Mineralogy and Petrology*, **116,** 433–447.

Holland, T. J. & Powell, R., 1998. An internally consistent thermodynamic data set for phases of petrologic interest. *Journal of Metamorphic Geology*, **16,** 309–343.

Johannes, W., 1983. On the origin of layered migmatites. In: *Migmatites, Melting and Metamorphism* (eds Atherton, M. P. & Gribble, C. D.), pp. 326. Shiva Publishing Limited, Nantwich, Cheshire, UK.

Jordan, P. G., 1988. The rheology of polymineralic rocks – an approach. *Geologische Rundshau*, **77,** 285–294.

Kohn, M. J. & Spear, F. S., 1990. Two new geobarometers for garnet amphibolites, with application to southeastern Vermont. *American Mineralogist*, **75,** 89–96.

Kopf, C., Williams, M., Snoeyenbos, D. & Hanmer, S., 1997. Heterogeneous metamorphism and deformation in an Archean lower-crustal shear zone; the Snowbird Tectonic Zone in northern Saskatchewan, Canada. *GAC/MAC Annual Meeting Abstracts*, **22,** A81.

Kretz, R., 1983. Symbols for rock-forming minerals. *American Mineralogist*, **68,** 277–279.

Lucas, S. B. & St-Onge, M. R., 1995. Syn-tectonic magmatism and the development of compositional layering, Ungava Orogen (northern Quebec, Canada). *Journal of Structural Geology*, **17,** 475–491.

MacKinnon, P., Fueten, F. & Robin, P.-Y. F., 1997. A fracture

model for quartz ribbons in straight gneisses. *Journal of Structural Geology*, **19,** 1–14.
Mader, U. K., Percival, J. A. & Berman, R. G., 1994. Thermobarometry of garnet–clinopyroxene–hornblende granulites from the Kapuskasing structural zone. *Canadian Journal of Earth Sciences*, **31,** 1134–1145.
Misch, P., 1968. Plagioclase compositions and non-anatectic origin of migmatitic gneisses in northern Cascades Mountains of Washington State. *Contributions to Mineralogy and Petrology*, **17,** 1–70.
Myers, J. S., 1978. Formation of banded gneisses by deformations of igneous rocks. *Precambrian Research*, **6,** 43–64.
Nekvasil, H. & Burnham, C. W., 1987. The calculated individual effects of pressure and water content on phase equilibria in the granite system. In: *Magmatic Processes: Physiochemical Principles* (ed. Mysen, B. O.), pp. 500. Geochemical Society, Pennsylvania.
Passchier, C. W. & Trouw, R. A. J., 1996. *Microtectonics*. Springer, Berlin.
Powell, R. & Holland, T. J. B., 1988. An internally consistent data set with uncertainties and correlations: 3. Applications to geobarometry, worked examples and a computer program. *Journal of Metamorphic Geology*, **6,** 173–204.
Ramberg, H., 1952. *The Origin of Metamorphic and Metasomatic Rocks*. University of Chicago Press, Chicago.
Robin, P.-Y. F., 1979. Theory of metamorphic segregation and related processes. *Geochimica et Cosmochimica Acta*, **43,** 1587–1600.
Rudnick, R. L., Fountain, D. & M., 1995. Nature and composition of the continental crust: a lower crustal perspective. *Reviews of Geophysics*, **33,** 267–309.
Simpson, C. & Wintsch, R. P., 1989. Evidence for deformation-induced K-feldspar replacement by myrmekite. *Journal of Metamorphic Geology*, **7,** 261–275.
Snoeyenbos, D. R., Williams, M. L. & Hanmer, S., 1995. Archean high-pressure metamorphism in the western Canadian shield. *European Journal of Mineralogy*, **7,** 1251–1272.
Spear, F. S., 1993. *Metamorphic Phase Equilibria and Pressure–Temperature–Time Paths*. Mineralogical Society of America.
Spry, A., 1969. *Metamorphic Textures*. Pergamon Press, Oxford.
Turner, F. J., 1941. The development of pseudo stratification by metamorphic differentiation in the schists of Otago, New Zealand. *American Journal of Science*, **239,** 1–16.
Turner, F. J. & Verhoogen, J., 1960. *Igneous and Metamorphic Geology*. McGraw-Hill, New York.
Van der Molen, I., 1985. Interlayer material transport during layer-normal shortening. part I. The model. *Tectonophysics*, **115,** 275–295.
Wen, S. & Nekvasil, H., 1994. Solvcalc: an interactive graphics program package for calculating the ternary feldspar solvus and for two-feldspar geothermometry. *Computers and Geosciences*, **2,** 1025–1040.
White, S. H., 1976. The effects of strain on the microstructures, fabrics, and deformation mechanisms in quartzites. *Philosophical Transactions of the Royal Society of London A*, **283,** 69–86.
Williams, M. L., Hanmer, S., Kopf, C. & Darrach, M., 1995. Syntectonic generation and segregation of tonalitic melts from amphibolite dikes in the lower crust, Striding-Athabasca mylonite zone, northern Saskatchewan. *Journal of Geophysical Research*, **100** (B8)**,** 15717–15734.
Yardley, B. W. D., 1989. *An Introduction to Metamorphic Petrology*. John Wiley & Sons, New York.

Received 30 November 1998; revision accepted 10 July 1999.